Palaeogeography, Palaeoclimatology, Palaeoecology 514 (2019) 98–108

Contents lists available at ScienceDirect

Palaeogeography, Palaeoclimatology, Palaeoecology

journal homepage: www.elsevier.com/locate/palaeo

Oligocene-Miocene (28–13 Ma) climato-tectonic evolution of the northeastern Qinghai-Tibetan Plateau evidenced by mineralogical and geochemical records of the Xunhua Basin

Zhao Liu[a,b], Hanlie Hong[a,*], Chaowen Wang[c], Wen Han[d], Ke Yin[a], Kaipeng Ji[a], Qian Fang[a], Thomas Algeo[e,f,g]

[a] School of Earth Sciences, China University of Geosciences, Wuhan 430074, China
[b] Gems and material technology Institute, Hebei GEO University, Shijiazhuang 050031, China
[c] Gemological Institute, China University of Geosciences, Wuhan 430074, China
[d] Beijing Institute of Gemology, National Gems & Jewelry Technology Administrative Center, Beijing 100013, China
[e] Department of Geology, University of Cincinnati, Cincinnati, OH 45221-0013, USA
[f] State Key Laboratory of Biogeology and Environmental Geology, China University of Geosciences, Wuhan 430074, China
[g] State Key Laboratory of Geological Processes and Mineral Resources, China University of Geosciences, Wuhan 430074, China

ARTICLE INFO

Keywords:
Clay minerals
Provenance
Laji Shan
Aridification
East Asian monsoon
Tectonic uplift

ABSTRACT

Changes in sediment composition in the Xunhua Basin provide insights into the climatic and tectonic evolution of the northeastern Qinghai-Tibetan Plateau during the Oligocene and Miocene. Here, we analyzed the clay mineralogy (i.e., the proportions of smectite, illite, and chlorite and clay indicators), bulk mineral composition (i.e., the amounts of calcite, quartz, gypsum, K-feldspar, plagioclase, dolomite, and halite), and trace-element indicators (i.e., Rb/Sr and Ba/Sr ratios) of sediments deposited from ~28 to 13 Ma in the Xunhua Basin to reveal the climate and/or provenance changes. The results suggest that significant changes in sediment provenance occurred at 25.1 Ma and 21.6 Ma, caused respectively by initial uplift and accelerated uplift of the Laji Shan. The Xunhua Basin experienced warm and humid conditions at 28.0–25.1 Ma, cool and dry conditions at 25.1–21.6 Ma, and somewhat warmer and wetter conditions at 21.6–19.2 Ma, followed by aridification in two steps at 19.2 Ma and 13.9 Ma. The climate cooling event at 25.1 Ma corresponds temporally to a major phase of uplift of central Tibet. Relatively warmer and wetter conditions during the early Miocene (21.6–19.2 Ma) are considered to record the influence of the Asian summer monsoon and accelerated uplift of the Laji Shan. The shift toward more arid conditions on the northeastern Qinghai-Tibetan Plateau at 19.2–13.9 Ma was probably driven by uplift of the Tibetan Plateau, and further aridification since 13.9 Ma may reflect a weakening of the East Asian summer monsoon and global climatic cooling.

1. Introduction

The Qinghai-Tibetan Plateau has undergone a complex tectonic and climatic evolution since the collision of India with southern Eurasia in the early Cenozoic (Harrison et al., 1992; Molnar et al., 1993, 2010; Molnar and Tapponnier, 1975). Tectonic studies from different parts of the plateau have suggested a wide range of uplift models and histories of plateau growth (Harrison et al., 1992; Molnar and Stock, 2009; Molnar et al., 1993; Tapponnier et al., 2001; C.W. Wang et al., 2008; S.F. Wang et al., 2008). Climatically, the appearance of the monsoonal system in East Asia and the onset of central Asian desertification is likely to have been related to Cenozoic Himalayan–Tibetan uplift and retreat of the Paratethys Sea (Clift et al., 2008; Guo et al., 2002, 2008; Ramstein et al., 1997; Sun and Wang, 2005; Zhang et al., 2007a, 2007b). Uplift of various parts of the Qinghai-Tibetan Plateau may also have differentially influenced the East Asian and Indian monsoons (Molnar et al., 2010; Xiao et al., 2012).

The northeastern margin of the Qinghai-Tibetan Plateau has received increasing attention, because it is important to investigate when and how the plateau grew northward, and it is within the transitional zone between humid areas to the east affected by the East Asian monsoon and arid areas to the west and, thus, sensitive to changes in the monsoonal climate (Dupont-Nivet et al., 2003, 2007, 2008b; Guo et al., 2002, 2008; Hough et al., 2011; Lu et al., 2004). Studies of

* Corresponding author.
E-mail address: honghl8311@aliyun.com (H. Hong).

https://doi.org/10.1016/j.palaeo.2018.10.009
Received 22 July 2018; Received in revised form 4 October 2018; Accepted 9 October 2018
Available online 13 October 2018
0031-0182/ © 2018 Elsevier B.V. All rights reserved.

magnetostratigraphy, biostratigraphy, clay mineralogy, stable isotopes, detrital AFT, and apatite fission-track thermochronology have been undertaken on various parts of the northeastern margin of the Qinghai-Tibetan Plateau, including the Xining Basin (Dai et al., 2006; Dupont-Nivet et al., 2004, 2008a; Horton et al., 2004; Xiao et al., 2012), Linxia Basin (Dettman et al., 2003; Hong et al., 2007; Fang et al., 2003; Garzione et al., 2005; Wang and Deng, 2005; Zheng et al., 2003), Guide Basin (Fang et al., 2005; Parés et al., 2003), and Lanzhou Basin (Li et al., 1997; Yue et al., 2001; Zheng et al., 2006). However, only a few studies have generated terrestrial climate records from the Asian interior that extend back to the early Miocene (e.g., Zhang et al., 2015). Palynological study of the Linxia Basin revealed a warm and humid climate at 21.8–18.6 Ma, a shift toward cooler conditions at 18.6–13 Ma, and aridification at 8.5–6 Ma (Ma et al., 1998). However, Guo et al. (2002) suggested that aridification of the northeastern Qinghai-Tibetan Plateau had commenced earlier, at ~22 Ma. The palynological record from the northern Tian Shan indicates wet conditions in central Asia during the late Oligocene and a shift to drier conditions at 23.8–23.3 Ma, which lessened during a relatively wet stage at 16.2 Ma (Tang et al., 2011).

The Xunhua Basin, located on the northeastern Qinghai-Tibetan Plateau, contains a continuous sequence of Cenozoic fluvial-lacustrine sediments (Xu et al., 2015) that preserve a relatively complete record of tectonic deformation and uplift, denudation and weathering history, and environmental and climatic changes on the northeastern plateau margin. Magnetostratigraphic studies have provided high-resolution dating of the Xunhua succession from ~30 Ma to ~5 Ma (Ji et al., 2010; Lease et al., 2012). Low-temperature thermochronometry studies have documented changes in provenance of sediments at ~22 Ma, coincident with accelerated growth of the Laji Shan, and at ~13 Ma, coincident with growth of the north-trending Jishi Shan (Fang et al., 2005; Lease et al., 2007, 2011, 2012). However, few studies have been undertaken to investigate the climate evolution and effects of differential uplift of the Qinghai-Tibetan Plateau on regional paleoclimate conditions. Clay-mineral studies can provide much useful information regarding topographic changes and their effects on climate and erosion rates (Hong et al., 2010). In this study, the mineralogical and geochemical characteristics of the Xunhua Basin succession were investigated to decipher their environmental significance, with the overall goal of obtaining a better understanding of the climatic and tectonic evolution of the northeastern Qinghai-Tibetan Plateau during the late Oligocene to middle Miocene.

2. Geological setting

The Xunhua Basin is located on the northeastern margin of the Qinghai-Tibetan Plateau (Fig. 1A), ~100 km southeast of Xining, Qinghai Province, China. The Xunhua Basin occupies a surface area of ~3300 km^2 with elevations ranging from 1870 m to 3000 m (Lease et al., 2012). The Xunhua Basin shows block faulting tectonic patterns typical of the northeastern Qinghai-Tibetan Plateau (Liu et al., 2007; Yin et al., 2010a, 2010b). Its northern border is the east-west-trending Laji Shan ("shan" = mountains), which separates the Xunhua Basin from the Xining Basin to the north. Its eastern border is the north-south-trending Jishi Shan, which separates the Xunhua Basin from the Linxia Basin to the east (Fig. 1B). Its western and southern borders are the Zhamazari Shan and West Qinling Mountains, respectively (Xu et al., 2015). The basement of the Xunhua Basin consists mainly of the Proterozoic Hualong Group, which contains schist, gneiss, marble, and amphibolite. The basin has accumulated a thick (to 2700 m) Cenozoic stratal succession that is dominated by fluvial and lacustrine redbed facies (Deng et al., 2000).

The Yangquangou section consists of outcrops in the southeastern Xunhua Basin, south of Xunhua town (section base: 35°49′30″N, 102°30′00″E; section top: 35°48′18″N, 102°16′10″E) and adjacent to the Yellow River (Fig. 1C). The ~1400-m-thick section comprises the Zhongzhuang (thickness: 930 m) and Shangzhuang formations (thickness: 468 m) and shows no evidence of sedimentary hiatuses. It contains four distinct lithofacies assemblages (Fig. 2). The first (the oldest) lithofacies assemblage, within the lower Zhongzhuang Formation (0–150 m), consists of gray-yellow medium-coarse conglomerate, pebbly coarse sandstone, and medium-coarse sandstone. The gravel clasts are 1.0–3.0 cm in diameter, poorly sorted, subrounded and imbricated. Tabular and trough cross-bedding, parallel bedding and scouring are widely present in the pebbly sandstone. Sedimentary facies of this unit are interpreted as braided stream deposits. The second lithofacies assemblage, within the middle to upper Zhongzhuang Formation (150–920 m), consists mainly of gray-green thinly bedded silty mudstone and gray-yellow mudstone interbedded with gypsum and interpreted as playa deposits. The third lithofacies assemblage, within the lower Shangzhuang Formation (920–1100 m), is dominated by sandy conglomerate, pebbly coarse sandstone, and muddy siltstone interbedded with planar medium to thick-bedded mudstones interpreted as deltaic deposits. Mudstone and silty mudstone beds with massive and asymmetric ripples are laterally continuous and accumulated rapidly on a delta front. Beds of conglomerate and pebbly coarse sandstone ranging from 3 to 5 m in thickness with parallel bedding and tabular and wedge-shaped cross-bedding accumulated as delta distributary channel deposits. The conglomerate clasts are usually medium-sorted, subangular to subrounded and imbricated. The fourth (the youngest) lithofacies assemblage, within the middle and upper part of the Shangzhuang Formation (1100–1400 m), is composed mainly of thinly bedded silty mudstone and mudstone interbedded with gypsum. Its characteristics are similar to the second unit and therefore interpreted as playa deposits.

Magnetostratigraphic study dated deposition of the Yangquangou section to ~28 to 13 Ma, with estimated ages for the Zhongzhuang and Shangzhuang Formations of ~28–19 Ma and ~19–13 Ma, respectively (Xu, 2015; Fig. 2). The Yangquangou section can be correlated to the nearby Xigou section (2 km distant) based on a distinctive gray-green sandstone layer. The Xigou section, which has yielded the vertebrates *Hipparion platyodus* Sefve and *Cervocerus* sp. indet., has a reported depositional age of 14.6–5.0 Ma (Ji et al., 2010; Xu et al., 2015). The *Hipparion* fossils in the Xunhua Basin, which are similar to fossils discovered in the northeastern Qinghai-Tibetan Plateau [Guide Basin (Fang et al., 2005; Parés et al., 2003; Song et al., 2003), Hualong Basin (Fang et al., 2003), Linxia Basin (Fang et al., 2003), and Guyuan Basin (Jiang et al., 2007)] and the southern Qinghai-Tibetan Plateau [Gyirong Basin (Yue et al., 2004) and Zanda Basin (C.W. Wang et al., 2008; S.F. Wang et al., 2008)]. According to magnetostratigraphic studies of these basins, the Hipparion fossils date to the middle Miocene to Pliocene (Xu et al., 2015).

3. Materials and methods

3.1. Samples

A total of 370 samples were collected at quasi-regular intervals of 3 to 4 m over a continuous stratigraphic interval of 1400 m spanning the Yangquangou section. Sampled lithologies include conglomerate, medium-coarse sandstone, fine sandstone, siltstone, and mudstone. Partial samples were selected according to lithological characteristics of detrital composition, grain size, and color for X-ray diffraction (XRD) and trace-element concentration measurements.

The study interval represents the upper Oligocene to middle Miocene (~28–13 Ma). Making use of fossil assemblages and magnetostratigraphic dating (Ji et al., 2010; Xu et al., 2015), the age of the section was refined through comparison with the recent geologic timescale of Gradstein et al. (2012) (Fig. 2). This analysis showed that the Zhongzhuang/Shangzhuang formation contact dates to C5Er (18.748–18.524 Ma), and that the major shifts in mineralogical and geochemical indicators at 245 m, 620 m, 862 m, and 1311 m can be

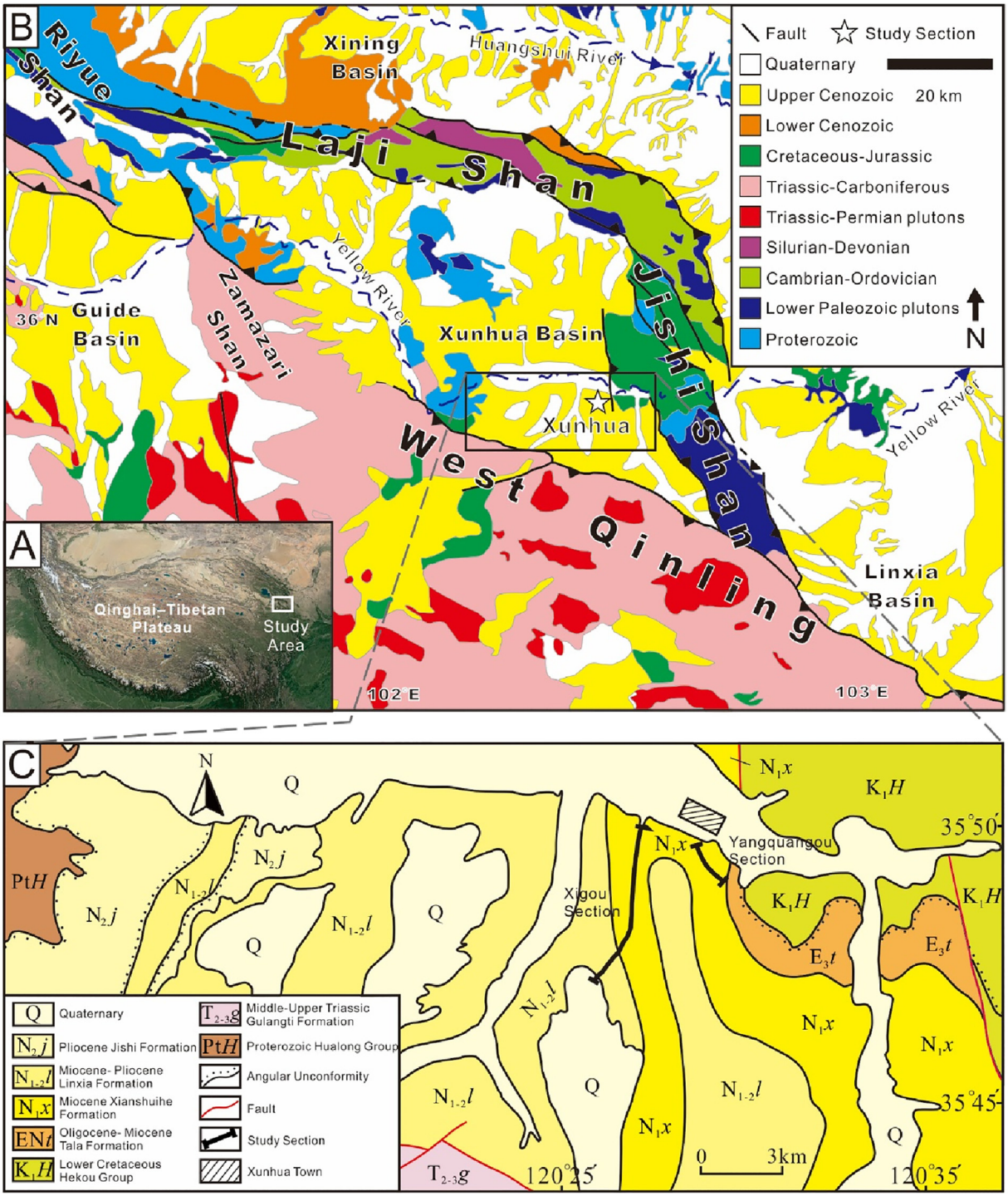

Fig. 1. (A) Location of the study area on Qinghai-Tibetan Plateau; (B) Regional geology of the Xunhua Basin (adapted from Lease et al., 2012); (C) Detailed geology and location of the study section (adapted from Ye et al., 2010).

assigned to C7Ar (25.099–24.984 Ma), C6AAn to C6AAr.2n (21.688–21.083 Ma), C6n (19.722–18.748 Ma), and C5ACn to C5ACr (14.163–13.739 Ma), respectively. In an age-thickness graph for the study section, these shifts are dated to 25.1, 21.6, 19.2, and 13.9 Ma, respectively (Fig. 3). Sedimentation rates for individual stratigraphic segments are mostly between 82 and 103 m/Myr, with an average sedimentation rate for the full section of ~93 m/Myr.

3.2. XRD analysis

A subset of 212 samples with the quasi-regular spacing of 5 to 8 m (corresponding to intervals of ~54–86 kyr) was selected for XRD measurements to determine the types and relative amounts of non-clay minerals. A fraction of each sample (about 200 g) was air-dried and ground to finer than 0.074 mm (Wang et al., 2013a, 2013b; Yin et al., 2013). The bulk mineral composition was identified by X-ray diffraction (XRD) using a Panalytical X' Pert PRO DY2198 diffractometer with Ni-filtered Cu Kα radiation (35 kV, 35 mA). The non-clay minerals calcite,

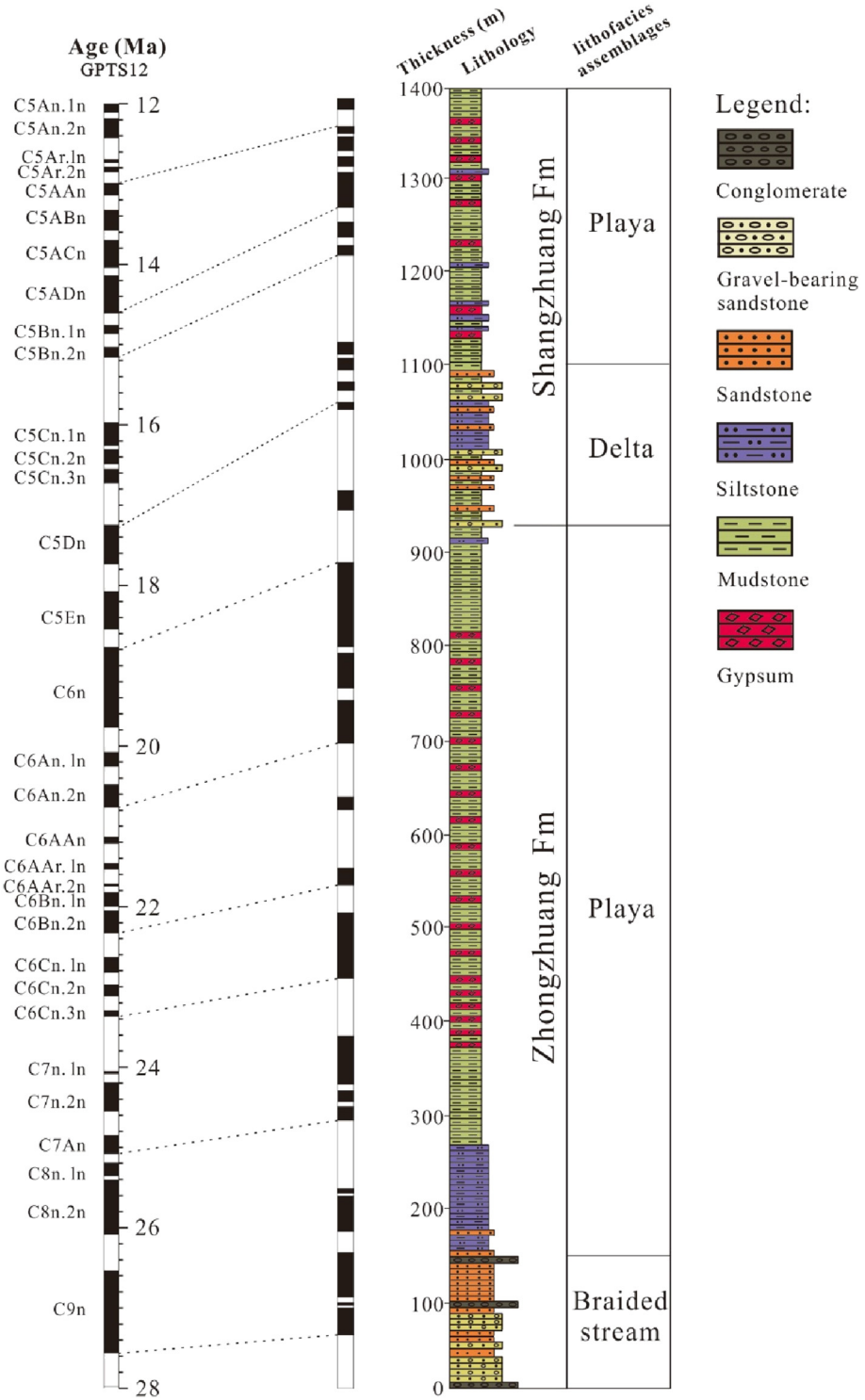

Fig. 2. Lithology, sedimentary facies and magnetostratigraphic results from the Yangquangou section, Xunhua Basin (cited from Xu, 2015), based on GPTS12 (Gradstein et al., 2012).

dolomite, quartz, gypsum, K-feldspar, plagioclase, and halite were identified by their characteristic peaks at 3.03, 2.89, 4.26, 7.60, 3.23, 3.18, and 2.82 Å, respectively, in X-ray diffractograms. The K-value method with reference material of corundum was used to determine the relative abundances of minerals in the bulk samples (Hong et al., 2010). The characteristic reflections of the above non-clay minerals to the (012) reflection of corundum at 3.48 Å were measured at 3.58, 3.58, 1.14, 3.00, 2.56, 2.25, and 6.29 Å, respectively (Hong et al., 2010; Wang et al., 2013a, 2013b). The detection limits were 1% for quartz and feldspar, 3% for calcite, and ~5% for other minerals (Ghandour et al., 2003).

A subset of 171 samples with the quasi-regular spacing of 7 to 9 m (corresponding to intervals of ~75–96 kyr) was selected for XRD measurements of clay minerals. Preparation of oriented clay samples and ethylene glycol (EG)-saturated clay samples followed the methods of Kahle et al. (2002) and Hong et al. (2007). Minerals were identified by characteristic reflections in X-ray diffractograms (Moore and Reynolds, 1989). The reflection peaks of smectite, illite, and chlorite in

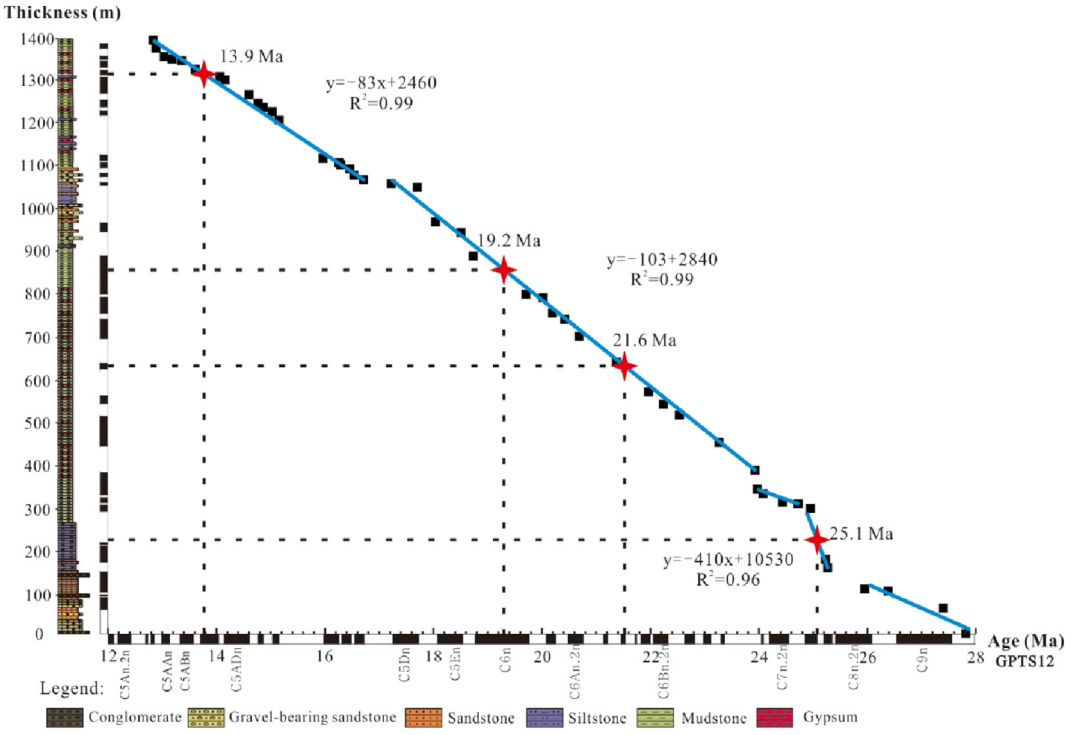

Fig. 3. Age-thickness graph showing major shifts at 245 m (25.1 Ma), 620 m (21.6 Ma), 862 m (19.2 Ma), and 1311 m (13.9 Ma).

the oriented clay samples were measured at 15.5, 10.0, and 3.52 Å, which changed to 17, 10, 3.52 Å after EG treatment (Hong et al., 2007; Hong et al., 2010; Wang et al., 2013a, 2013b). The integrated peak areas of EG-treated samples were used to determine the relative abundances of the clay-mineral fractions (Biscaye, 1965). The relative abundances of clay minerals were determined using the formula: 4 × I (illite-10 Å) + I (smectite-17 Å) + 2 × I (chlorite-3.52 Å) = 100% (Hong et al., 2010), and the (chlorite + illite)/smectite ratio was calculated based on the relative abundances of the clay minerals. Illite crystallinity (IC) values were obtained from the half-height width of the 10-Å peak in EG-saturated patterns; note that high (low) values indicate low (high) crystallinity.

3.3. Major and trace-element concentration analysis

A subset of 84 samples with the quasi-regular spacing of 15 to 18 m (corresponding to intervals of ~160–190 kyr) was selected for major and trace element analysis. Carbonate and organic carbon were removed from the bulk sample through digestion in 1 M acetic acid and 30% H_2O_2, respectively (Xiong et al., 2010). The purpose of this step was to isolate the siliciclastic fraction for analysis of chemical weathering intensity. The samples were then dried and sieved to pass through a 1 mm nylon sieve, followed by grinding to 200 mesh (< 0.074 mm). The purpose of these steps was to recover a standard (fine) grain-size fraction to limit the influence of grain size on chemical weathering proxies (Zhang et al., 2002).

Major-element concentrations were determined by X-ray fluorescence (XRF) spectrometry in the State Key Laboratory of Biogeology and Environmental Geology using a Shimadzu XRF-1800 sequential spectrometer. The loss-on-ignition (LOI) value was calculated from the difference in mass after sample heating to 105 °C and 950 °C. The analytical precision for major-element concentrations was < 1% and the detection limits were 0.01%. Trace element concentrations (including Rb, Ba, and Sr) were determined using an Agilent 7700e ICP-MS. The analytical precision and accuracy were better than ± 2% (cf. Liu et al., 2008).

The chemical index of alteration (CIA) was proposed to evaluate the weathering intensity of samples (Nesbitt and Young, 1982):

$$CIA = Al_2O_3/(Al_2O_3 + CaO^* + Na_2O + K_2O) \quad (1)$$

in which elemental abundances are expressed as molar proportions, and CaO* represents the Ca associated with silicate minerals. Because the samples contain calcite and dolomite, CaO* was modified according to McLennan (1993): if the molar proportion of CaO is less than that of Na_2O, CaO* is equal to CaO, but otherwise it is equal to Na_2O. Rb/Sr and Ba/Sr were calculated as weight ratios.

4. Results

X-ray diffraction data show that the relative proportions of the clay and non-clay fractions of most samples are relatively uniform. The main non-clay minerals are quartz, feldspars (plagioclase and K-feldspar), calcite, dolomite, gypsum, and minor halite, and the main clay minerals are illite, smectite, and chlorite (Figs. 4, 5). Kaolinite is not reported because of its small quantity (not detected by XRD) in the study samples.

The relative proportions of different non-clay minerals vary markedly among samples (Fig. 4). Quartz and feldspar, which represent the weathering products of various sedimentary, metamorphic, and volcanic rocks from the surrounding mountains (Wang et al., 2013a, 2013b), are the dominant minerals through most of the profile, with contents of 19–65% (mean 44%) and 1–41% (mean 12%), respectively. Gypsum and halite have total contents of 2–77% (mean 33%). Calcite and dolomite occur sporadically, with contents of 0.3–42% (mean 8%) and 0–29% (mean 3%), respectively (Fig. 4). As for clay minerals, illite, smectite, and chlorite are ubiquitous throughout the study section, with contents of 42–69% (mean 61%), 10–42% (mean 16%), and 13–28% (mean 23%), respectively (Fig. 5a–c). Illite crystallinity spans 0.19–0.53°2Θ, averaging 0.354, showing a decreasing trend from the bottom to top (Fig. 5g). Rb/Sr and Ba/Sr ratios range from 0 to 1.4 (mean 0.25) and from 0 to 3.9 (mean 1.05), respectively. CIA values are between 58 and 73 (mean 66; Fig. 6), indicating that the chemical weathering intensity of the source materials was intermediate (Fedo et al., 1995).

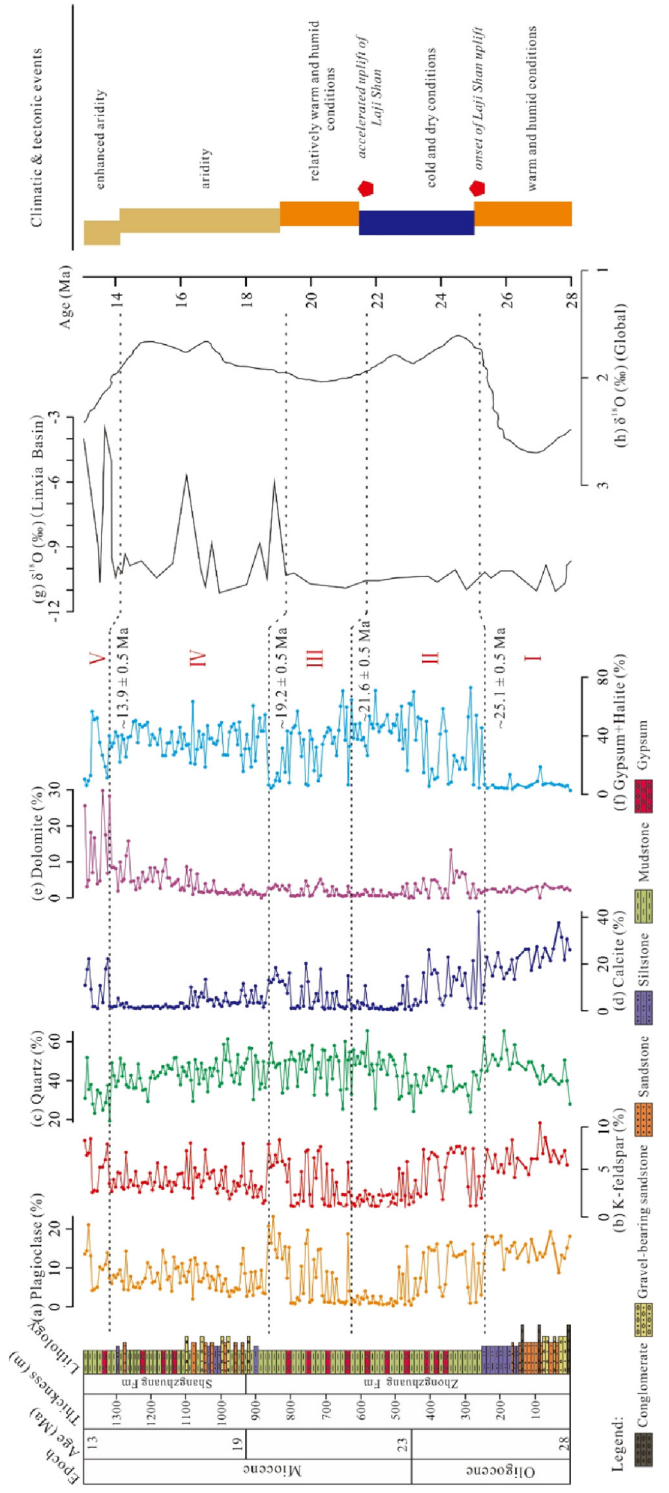

Fig. 4. Variations of bulk mineral content in Xunhua Basin, $\delta^{18}O$ data from Linxia Basin (Dettman et al., 2003) and globally (Zachos et al., 2001), and climatic and tectonic events in Xunhua Basin from Oligocene to Miocene (~28–13 Ma).

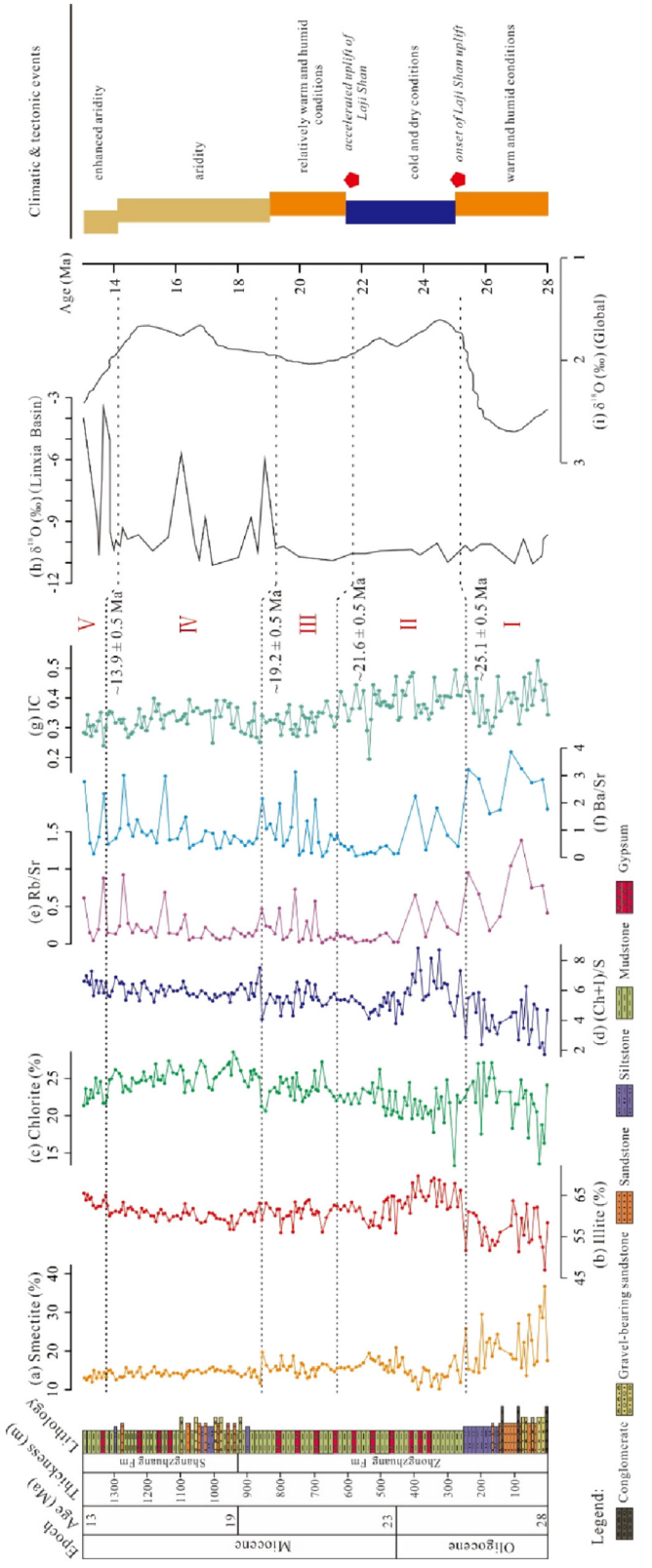

Fig. 5. Variations of clay mineral contents, trace geochemical proxies and illite crystallinity from Xunhua Basin, $\delta^{18}O$ data from Linxia Basin (Dettman et al., 2003) and globally (Zachos et al., 2001), and climatic and tectonic events in Xunhua Basin from Oligocene to Miocene (~28–13 Ma).

The study interval can be subdivided into five units according to different lithofacies and compositional characteristics: Unit I (28–25.1 Ma), Unit II (25.1–21.6 Ma), Unit III (21.6–19.2 Ma), Unit IV (19.2–13.9 Ma), and Unit V (13.9–13 Ma) (Figs. 4, 5). In Unit I, plagioclase and K-feldspar contents are high, and gypsum + halite and dolomite contents are stable and low. Quartz content increases upsection, whereas calcite is initially high and decreases upsection. The contents of smectite, illite, and chlorite all have relatively large amplitudes of variation. The (chlorite + illite)/smectite ratio and illite and chlorite contents increase and smectite decreases upsection. Rb/Sr and Ba/Sr

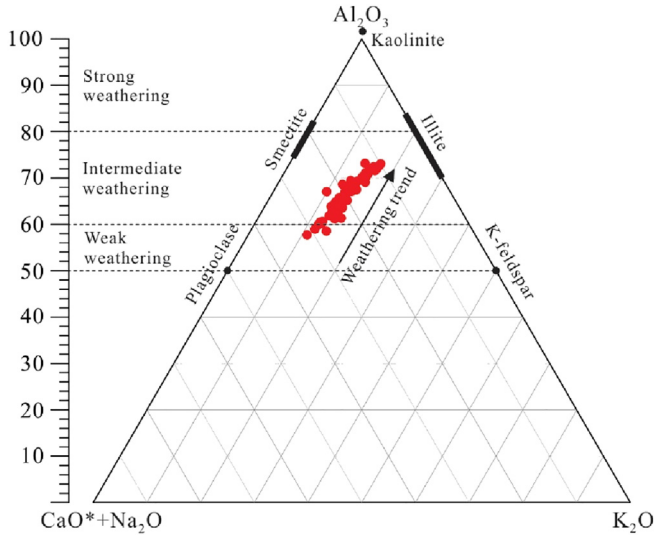

Fig. 6. Chemical index of alteration (CIA) for Xunhua Basin sediments.

ratios also vary strongly but show a generally decreasing trend upsection. In Unit II, plagioclase, K-feldspar, and quartz content decrease sharply upsection, but gypsum + halite content increases. Dolomite content is relatively high. Illite content and (chlorite + illite)/smectite ratio show increasing trends upsection, whereas calcite, smectite, and chlorite contents and Rb/Sr and Ba/Sr ratios decrease upsection. In Unit III, the contents of plagioclase, K-feldspar, calcite, and smectite, and Rb/Sr, Ba/Sr ratios increase upsection, whereas the contents of gypsum + halite, illite, and chlorite and (chlorite + illite)/smectite ratio decrease. Quartz and dolomite contents are generally stable. The Unit III/IV contact coincided with a pronounced shift in almost all indicators. In Unit IV, most indicators exhibit relatively stable values, but calcite content decreases and dolomite content increases upsection. In Unit V, the contents of plagioclase, K-feldspar, calcite, dolomite, illite, and gypsum + halite and the ratios of Rb/Sr, Ba/Sr, and (chlorite + illite)/smectite show increasing trends upsection, whereas the contents of quartz, chlorite, and smectite decreased.

5. Discussion

Firstly, we discuss interpretations of the geochemical and mineralogical proxies for bulk sample and clay fraction data in the Yangquangou section of the Xunhua Basin. Secondly, we discuss the pronounced changes in sediment provenance and climate conditions at 25.1, 21.6, and 19.2 Ma that can be inferred from analysis of these records.

5.1. Interpretation of environmental and provenance proxies

Climate controls rainfall and temperature, which strongly influence chemical reaction rates (West et al., 2005). Higher rainfall and temperatures generally enhance chemical reaction, leading to more highly weathered sediment compared to cool, dry climates. These processes largely control sedimentary mineral associations. Lakes in arid climates commonly accumulate halite and gypsum, especially during drawdown stages (Dupont-Nivet et al., 2007). Climate cooling/drying and warming both favor the deposition of halite and gypsum via a decrease in freshwater supply and an increase in lake-surface evaporation (Wang et al., 2013a). Illite is an indicator for mechanical erosion and less chemical weathering product of aluminosilicate minerals either under a dry and cool climate or a consequence of a pronounced relief (Grim, 1968). Chlorite is preserved under an arid climate and is usually derived from metamorphic rocks, especially of greenschist facies (Ducloux et al., 1976; Vanderaveroet, 2000). Illite and chlorite are the direct weathering products of parent rocks that have experienced limited leaching (Robert and Kennett, 1994). During pedogenesis under warm and humid climate conditions, chlorite and illite can transform to smectite or even kaolinite (Vicente et al., 1997; Hong et al., 2007).

Weathering can result in major changes of sedimentary elemental ratios, such as Rb/Sr and Ba/Sr, because Sr is susceptible to loss to solution, whereas Rb and Ba in soil waters have a strong tendency to be adsorbed onto clay minerals (Buggle et al., 2011). Under extreme chemical weathering conditions, K, Rb, Ba will become strongly depleted (Condie et al., 1995). However, variation of Ba/Sr and Rb/Sr ratios can also result from changes in the provenance of weathering fluxes. For example, the addition of feldspar can increase these ratios because feldspar is rich in Ba and Rb (Zhang et al., 2002), whereas reworking of secondary carbonate can reduce these ratios because carbonate is rich in Sr (Buggle et al., 2011). Therefore, changes of climate and sediment provenance are key factors in interpreting secular variation in chemical weathering proxies.

Apart from climate and provenance changes, sedimentary mineral associations and chemical weathering indicators can also be influenced by diagenesis and the grain size of samples (Fralick and Kronberg, 1997). During diagenesis, smectite can transform to illite, with mixed-layer illite-smectite as an intermediate phase, at temperatures within the oil window (Perry and Hower, 1970). However, the study units contain discrete clay-mineral phases (e.g., smectite, illite, chlorite and kaolinite) with no occurrence of mixed-layer illite-smectite. Moreover, diagenesis will result in an increase of illite content and decrease of IC values with depth in the profile (Drits et al., 2002; Warr and Rice, 1994). Overall, IC values and illite contents show trends opposite to those expected if diagenesis were the dominant control on these parameters (Fig. 5b, g). Furthermore, the sandstones and mudstones exhibit an unconsolidated texture with poor cementation. Samples were prepared by chemical removal of carbonate and organic matter, and by sieving to achieve a uniform grain size, in order to minimize grain-size effects. Therefore, diagenesis and grain size likely were negligible influences on the mineral assemblages and elemental ratios in this study.

5.2. Climatic and tectonic evolution of the Xunhua Basin

A major shift in the contents of clay minerals and gypsum + halite within the study section occurred at 25.1 Ma (late Oligocene), likely due to climate change. During deposition of Unit I (28–25.1 Ma), the climate of the Xunhua Basin was warm and humid, with relatively intense chemical weathering. This condition is evidenced by high smectite content, low illite and gypsum + halite contents, and low (chlorite + illite)/smectite ratios. However, during deposition of Unit II (25.1–21.6 Ma), increases in illite content and (chlorite + illite)/smectite ratio together with decreases in smectite content indicate climatic cooling and drying. Climate cooling and drying at 25.1–21.6 Ma are reinforced by changes in evaporite minerals, i.e., a sharp increase in gypsum + halite content.

Rapid changes in plagioclase, K-feldspar, quartz, and calcite contents occurred at 25.1 Ma, indicating a change of sediment provenance. Although climate was the dominant control on sediment composition during deposition of Unit II, changes in sediment provenance were also important. Plagioclase, K-feldspar, quartz, and calcite contents show decreasing trends that may reflect a shift toward sources areas with lower contents of these minerals, although some of the decrease was due to a concurrent increase in the amounts of gypsum + halite. The significant shifts in plagioclase, K-feldspar, quartz, and calcite contents (Fig. 4a–d) indicate a change in sediment provenance at 25.1 Ma. Furthermore, chlorite content decreased at this time owing to climatic cooling and drying, which is counter-intuitive given that its low resistance to hydrolysis generally causes chlorite content to increase under cool-dry conditions (Robert and Kennett, 1997). Chlorite is a useful proxy for physical weathering in source regions as it is derived mainly via mechanical erosion of low- and medium-grade metamorphic

rocks (Hurlbut and Klein, 1985).

These mineralogical changes can be interpreted as a change of provenance from predominantly West Qinling Mountains sources to a mixture of West Qinling Mountains and East Laji Shan sources. This inference is supported by geological and paleocurrent data (Xu et al., 2015). Analysis of imbricate gravels at the base of the Zhongzhuang Formation indicates western to northwestern paleocurrent flow and a source terrain composed of sandstone, matasandstone, limestone, monocrystalline quartz, granite, and minor slate and chert. However, paleocurrent flow changed to a southern to southwestern direction, and the source material to andesite, granite, quartzite, sandstone and chert in the middle of Zhongzhuang Formation. Geologic mapping shows that the northern margin of the West Qinling Mountains consists mainly of Triassic flysch, siliceous mudstone, and limestone (Lease et al., 2012), whereas the East Laji Shan consists of Upper Devonian intermediate-basic volcanic rock, volcaniclastic rock, and siliceous mudstone (Liu et al., 2007). The composition of gravel at the base of the Zhongzhuang Formation is consistent with a source on the northern margin of the West Qinling Mountains, whereas that from the middle of the Zhongzhuang Formation suggests a mixture of eroded material from the West Qinling Mountains and the East Laji Shan.

Both climatic cooling and drying and provenance changes favored decreases in Rb/Sr and Ba/Sr at 25.1 Ma. In view of decreases in feldspar and carbonate content at 25.1 Ma, lowered Rb/Sr and Ba/Sr ratios may have been caused mainly by a sharp decline in inputs of feldspar. Climatic cooling and drying decreased the leaching of Sr to a minimum, contributing to the decreases of Rb/Sr and Ba/Sr. In summary, comparison of Unit I and Unit II shows that the climate shift from warm and wet (within 28–25.1 Ma interval) to cool and dry (within 25.1–21.6 Ma interval) was accompanied by a major provenance change at 25.1 Ma.

Another significant shift in the geochemistry and mineralogy of the study section at 21.6 Ma (Unit II/III transition) is interpreted as due to a shift in sediment provenance driven by contemporaneous climate change. At that time, the climate of the Xunhua Basin became warmer and more humid, as reflected in changes in evaporite mineral content and Rb/Sr and Ba/Sr ratios. During deposition of Unit III (21.6–19.2 Ma), increases of Rb/Sr and Ba/Sr and a slight decrease of gypsum + halite content may have been related to intensified weathering of silicates and increased freshwater influx, respectively (Wang et al., 2013a, 2013b).

Sediment provenance may have been more important than climate in controlling compositional changes during this interval, however. The contents of plagioclase, K-feldspar and calcite show significant increases (Fig. 4a–b, d) suggesting that sediment provenance within the Xunhua Basin changed at 21.6 Ma. The contents of feldspars (plagioclase and K-feldspar) and calcite increased, indicating the new source area yielded more of these minerals. The West Laji Shan, which is relatively far from the Xunhua Basin, consists mainly of Mesoproterozoic slate, phyllite, and limestone (Liu et al., 2007). We interpret the provenance change in the Xunhua Basin after 21.6 Ma as likely related to uplift of the West Laji Shan. Thus, sediment provenance changed from dominantly West Qinling and East Laji Shan sources to a mixture that included inputs from the West Laji Shan. Low-temperature thermochronometry confirmed accelerated exhumation of the Laji Shan at ~22 Ma (Lease et al., 2012). A provenance change is supported by increasing chlorite content at 21.6 Ma, a pattern that is unlikely to have been due to climate change because a warmer and wetter climate should have reduce chlorite content. The slightly decreasing trends of illite and (chlorite + illite)/smectite ratio are in line with the increasing trends of feldspars, calcite and Rb/Sr, Ba/Sr ratios (Figs. 4a–b, d, and 5d–f). Higher Rb/Sr and Ba/Sr ratios were controlled to a large degree by the increase of feldspars. Variations of all indicators indicate that provenance changes were important in the Xunhua Basin at 21.6–19.2 Ma. All observations suggest that provenance changes caused by accelerated exhumation of the Laji Shan were the dominant factor and that a warmer and more humid climate was a secondary influence on sediment composition in the Xunhua Basin during 21.6–19.2 Ma.

At the onset of deposition of Unit IV (19.2 Ma), shifts in the majority of indicators indicate that Xunhua Basin sediments experienced a major climate change. An increase in chlorite content and (chlorite + illite)/smectite ratio, a decrease of smectite content, and lower Rb/Sr and Ba/Sr ratios suggest that the climate changed to much drier and cooler conditions. These results are in accordance with a pronounced increase in gypsum + halite content that is interpreted as due to intense aridification of the Xunhua Basin at 19.2 Ma. Concurrent declines in the contents of plagioclase, K-feldspar, quartz, calcite, and dolomite reflect the large increase of gypsum + halite content. Further evidence for aridification of the NE margin of the Qinghai-Tibetan Plateau at 19.2 Ma is provided by the $\delta^{18}O$ record of the Linxia Basin (Dettman et al., 2003) and the clay-mineral index of the Xining Basin (Zhang et al., 2015), to the east of the Xunhua Basin (Figs. 4g, 5h).A decrease in calcite and increase in dolomite content during the latter part of Unit IV deposition reflects dolomitization of calcite. The formation of dolomite requires permeability, a mechanism that facilitates fluid flow, and a sufficient supply of magnesium (Warren, 2000). Increasing dolomite content in the Xunhua Basin was linked to a change from delta to playa facies, which was more favorable for dolomite formation, and to a relatively warm and humid climate (Wang et al., 2013a, 2013b). Provenance changes seem to have been unimportant in the Xunhua Basin at 19.2 Ma. Even though quartz content increased significantly at 19.2 Ma, the contents of plagioclase, K-feldspar, and calcite were relatively stable (Fig. 4a, b, c, d) from 19.2 to 13.9 Ma, suggesting minimal provenance changes.

5.3. Relationship of regional environmental change and East Asian monsoon evolution

Tectonic uplift of the mountains surrounding the Xunhua Basin during the late Oligocene to middle Miocene triggered major changes in regional climate and sediment sources. Subsidence and fill of the Xunhua Basin was closely related to the uplift histories of the West Qinling Mountains, Laji Shan, and Jishi Shan (Ji et al., 2010; Lease et al., 2007, 2011, 2012; Xu, 2015; Xu et al., 2015). Orogenic uplift is evidenced by a change in sediment provenance at ~25.1 Ma in the Xunhua Basin (this study) and by a similar change in the Xining Basin to the north of the Xunhua Basin at ~25 Ma (Xiao et al., 2012). We infer that these changes in sediment provenance were caused by initial uplift of the Laji Shan, which is located between the Xunhua and Xining basins.

The change in sediment provenance at ~25.1 Ma was associated with climatic cooling and drying, as indicated by increased gypsum content and changes in clay-mineral assemblages, e.g., increased illite content and decreased smectite and chlorite contents. In the Linxia Basin to the east of the Xunhua Basin, clay-mineral assemblages and carbon isotopic data reveal a warm and seasonally humid climate from ~29 Ma to ~24 Ma, followed by a gradual cooling and drying trend after ~24 Ma (Dettman et al., 2003; Hong et al., 2007). The similarity of compositional trends in the Xunhua and Linxia basins suggests that common climatic changes occurred across the northeastern Qinghai-Tibetan Plateau region during this period.

Large-scale uplift of central Tibet since ~26 Ma affected climates regionally by blocking transport of tropical moisture (DeCelles et al., 2007), resulting in reduced rainfall on the northeastern margin of the Qinghai-Tibetan Plateau (Hong et al., 2007). Tectonically forced climatic cooling of the northern Tibetan Plateau during the Eocene-Miocene (Fig. 7) has been recognized in the western Tarim Basin, the Altyn Tagh region, and the Qilian Shan (Cowgill et al., 2003; George et al., 2001; Jolivet et al., 2001; Mock et al., 1999; Sobel and Dumitru, 1997). Thus, the pattern of climate change in the Xunhua Basin at 25.1–21.6 Ma was likely linked to major uplift of central Tibet during the latest Oligocene to earliest Miocene (Fig. 7).

Accelerated uplift of the Laji Shan began at ~22 Ma, as

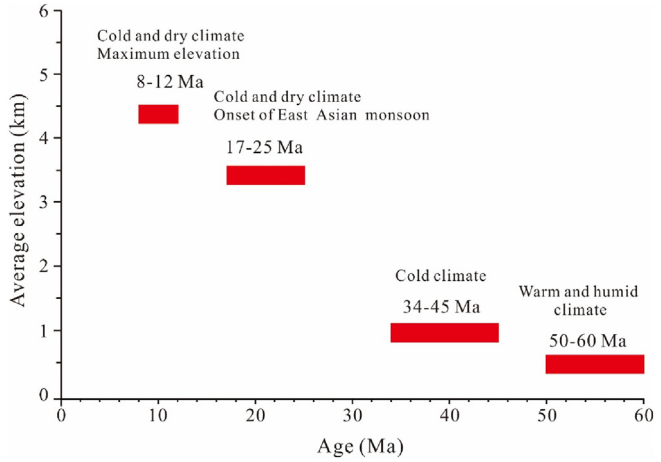

Fig. 7. Elevations versus time for the Tibetan Plateau (cited from Zhang et al., 2013). Data sources for Qinghai-Tibetan Plateau uplift at 25–17 Ma: George et al. (2001); Sobel et al. (2006); Wang (2013); Yin et al. (1998, 2007).

demonstrated by low-temperature thermochronometry (Lease et al., 2011, 2012) and magnetostratigraphic studies (Xiao et al., 2012). This event increased the flux of weathered materials and altered sediment sources to the Xunhua Basin, recorded in changes in feldspar, calcite and chlorite contents at 21.6 Ma. In addition to decreases in gypsum +halite content and changes in clay-mineral assemblages, several lines of evidence indicate a relatively warmer and wetter climate at 21.6–19.2 Ma. Palynological studies reveal a change in vegetation types within the Xunhua Basin, from conifer forests to mixed broadleaf-conifer forests, after ~23 Ma (Xu, 2015). Warm and wet conditions at 22.0–19.7 Ma are also evidenced by chromaticity (a*/L*) data from the QA-I (Qinan) section (Guo et al., 2008) and a humidity index from the Sikouzi section of the Xining Basin (Jiang and Ding, 2008; Wang et al., 2011). Further afield, marine oxygen isotope and atmospheric CO_2 data (Zachos et al., 2001, 2008; Figs. 4h, 5i) reflect relatively warm and humid conditions during the early Miocene that have been attributed to the initial organization of the East Asian monsoon system (Guo et al., 2002, 2008). Thus, increasingly warm and humid conditions at 21.6–19.2 Ma reflect the growing influence of the Asian summer monsoon on the Xunhua Basin.

The Xunhua Basin experienced increasingly arid conditions after 19.2 Ma. To obtain a better understanding of early Miocene climatic changes in central Asia, we compared the Yangquangou section record with other continental records from the northeastern Qinghai-Tibetan Plateau. A $\delta^{18}O$ profile from the Linxia Basin shows a sharp increase at 19.2 Ma, reflecting climate aridification (Dettman et al., 2003). The palynology of the Maogou section from the nearby Linxia Basin shows a shift toward warmer and wetter conditions at 21.8–18.6 Ma followed by long-term drying at 18.6–13.0 Ma (Ma et al., 1998). Sedimentological, mineralogical, and geochemical proxies from the TS section in the Xining Basin indicate increasing aridity after ca. 19.7 Ma (Zhang et al., 2015). The pollen record from the Sikouzi section in Guyuan suggests a gradual drying trend after ~19.7 Ma (Jiang and Ding, 2008; Wang et al., 2011; Zhang et al., 2015). Clay-mineral assemblages from the Xinghai Basin to the west of the Xunhua area reflect increasing aridification after ~19.7 Ma (Wang, 2015). Collectively, these studies document increasing aridification broadly across the northeastern Qinghai-Tibetan Plateau after ~19 Ma, in good agreement with observations for the Xunhua Basin in the present study.

The long-term aridification of central Asia during the late Neogene has been attributed to a combination of global and regional factors, including global climatic cooling (Dupont-Nivet et al., 2007; Liu and Ding, 1998; Miao et al., 2012) and uplift of the Tibetan Plateau (An et al., 2001; Manabe and Terpstra, 1974; Ruddiman and Kutzbach, 1989; Zhang et al., 2015). Global deep-sea $\delta^{18}O$ (Figs. 4h, 5i) and atmospheric CO_2 records show that the early Miocene climate was stable and warm after ~22 Ma (Miller et al., 2005; Zachos et al., 2001, 2008; Zhang et al., 2015), and particularly during the Mid-Miocene Climate Optimum (17–14 Ma) (Escutia et al., 2005;Flower and Kennett, 1994; Jiménez-Morenoa et al., 2005; Sun and Zhang, 2008; Utescher et al., 2000). Thus, evidence for dry conditions on the northeastern Qinghai-Tibetan Plateau during this interval does not agree with global trends, suggesting that global climatic changes were not a major factor in the gradual aridification of this region after 19.2 Ma. Thus, uplift of the Tibetan Plateau was the most likely cause of aridification of the northeastern Qinghai-Tibetan Plateau during the early to middle Miocene.

Multiple records from different regions of the northeastern Qinghai-Tibetan Plateau document enhanced aridity after 13.9 Ma. Increasing aridity in the Xunhua Basin at that time is shown by changes in clay mineralogy, bulk mineral composition, and trace-element indicators. This event was also recorded by pollen data from the Xunhua Basin, which show a sharp increase in xerophytic taxa and a reduction in thermophilic taxa at ~13.6 Ma (Xu, 2015). The $\delta^{18}O$ values of lake carbonates in the Linxia Basin increase after 14.0 ± 0.5 Ma, representing more arid conditions (Figs. 4g, 5h Dettman et al., 2003). The Miocene chromaticity record (a*/L*) from bulk sediments of the QA-I (Qinan) section exhibits a large decrease at ~13.5 Ma, indicating a shift to more arid conditions (Guo et al., 2008). Pollen data from the Sikouzi section in the Ningxia Basin reflect a major decline in East Asian summer monsoon intensity during the interval from 14.25 to 11.35 Ma (Jiang and Ding, 2008).

Increasing aridification of the northeastern Qinghai-Tibetan Plateau after 13.9 Ma was most likely the result of a decline in intensity of the East Asian summer monsoon together with global climatic cooling. Intensified uplift of the Himalayan-Tibetan Plateau after ~14 Ma (i.e., in the mid-Miocene) strongly reduced moisture transport to the Asian interior (Coleman and Hodges, 1995; Guo et al., 2008; Spicer et al., 2003; Turner et al., 1993). Global cooling after ~14 ± 0.5 Ma (Figs. 4h, 5i), which has been documented by global deep-sea oxygen and carbon isotope records (Zachos et al., 2001, 2008), may also have contributed to aridification of the Xunhua Basin.

6. Conclusions

Investigation of the upper Oligocene-middle Miocene sedimentary sequence in the Xunhua Basin of the northeastern Qinghai-Tibetan Plateau reveals shifts in bulk mineralogy and clay-mineral assemblages that reflect major changes in climate and sediment provenance from ~28 Ma to ~13 Ma. Significant changes in sediment provenance occurred at 25.1 Ma and 21.6 Ma caused, respectively, by initial uplift and accelerated uplift of the Laji Shan. The Xunhua Basin experienced warm and wet conditions at 28–25.1 Ma, but shifted to cooler and drier conditions at 25.1–21.6 Ma. A second phase of relatively warmer and wetter conditions followed at 21.6–19.2 Ma, which was terminated by stepwise intensification of aridity at 19.2 Ma and 13.9 Ma. The climate event at ~25.1 Ma coincided with a major stage of uplift of central Tibet, reflecting tectonic forcing of climatic cooling. The early Miocene warm-wet phase at ~21.6–19.2 Ma was influenced by the Asian summer monsoon as well as by accelerated uplift of the Laji Shan. Increasing aridity on the northeastern Qinghai-Tibetan Plateau at 19.2–13.9 Ma was most likely driven by uplift of the Tibetan Plateau, and enhanced aridity after ~13.9 Ma reflected a combination of declining intensity of the East Asian summer monsoon and global climatic cooling.

Acknowledgments

This work was supported by the Key Project Foundation of China Geological Survey (No. 1212011121261), NSFC (Nos. 41272053,

41472041, 41402036 and 41602037), NSF of Hubei for Young Scholars (2016CFB183), Jiangsu Postdoctoral Science Foundation of China (2015M582301), and Fundamental Research Funds for Central Universities (Wuhan, CUG160848). We hereby give our thanks to Prof. Kexin Zhang, Zenglian Xu, Feng Cheng, Zhiming Zhang, Fan Zhang, Yao Xiao, Fei Hu and Songfeng Liu for their participation in field work, samples measurements, and figures drawing.

References

An, Z.S., Kutzbach, J.E., Prell, W.L., Porter, S.C., 2001. Evolution of Asian monsoons and phased uplift of the Himalaya–Tibetan plateau since Late Miocene times. Nature 411, 62–66.

Biscaye, P.E., 1965. Mineralogy and sedimentation of recent deep-sea clays in the Atlantic Ocean and adjacent seas and oceans. Geol. Soc. Am. Bull. 76, 803–832.

Buggle, B., Glaser, B., Hambach, U., Gerasimenko, N., Marković, S., 2011. An evaluation of geochemical weathering indices in loess–paleosol studies. Quat. Int. 240, 12–21.

Clift, P.D., Hodges, K.V., Heslop, D., Hannigan, R., Van Long, H., Calves, G., 2008. Correlation of Himalayan exhumation rates and Asian monsoon intensity. Nat. Geosci. 1 (12), 875–880.

Coleman, M., Hodges, K., 1995. Evidence for Tibetan plateau uplift before 14 Myr ago from a new minimum age for east-west extension. Nature 374, 49–52.

Condie, K.C., Dengate, J., Cullers, R.L., 1995. Behavior of rare earth elements in a paleoweathering profile on granodiorite in the Front Range, Colorado, USA. Geochim. Cosmochim. Acta 59, 279–294.

Cowgill, E., Yin, A., Harrison, T.M., Wang, X.F., 2003. Reconstruction of the Altyn Tagh fault based on U-Pb geochronology: role of back thrusts, mantle sutures, and heterogeneous crustal strength in forming the Tibetan Plateau. J. Geophys. Res. 108 (B7) (#2346, 28 pp.).

Dai, S., Fang, X., Dupont-Nivet, G., Song, C., Gao, J., Krijgsman, W., Langereis, C., Zhang, W., 2006. Magnetostratigraphy of Cenozoic sediments from the Xining Basin: tectonic implications for the northeastern Tibetan Plateau. J. Geophys. Res. 111 (B11102) (19 pp).

DeCelles, P.G., Quade, J., Kapp, P., Fan, M., Dettman, D.L., Ding, L., 2007. High and dry in central Tibet during the Late Oligocene. Earth Planet. Sci. Lett. 253, 389–401.

Deng, Z.L., Hou, Y., Gu, F., 2000. Filling characteristics, sporopollen assemblage and paleoclimate variation of tertiary basins in the northeastern Qinghai-Tibetan Plateau. Qinghai Geol. 1, 43–53 (in Chinese).

Dettman, D.L., Fang, X., Garzione, C.N., Li, J., 2003. Uplift-driven climate change at 12 Ma: a long ^{18}O record from the NE margin of the Tibetan Plateau. Earth Planet. Sci. Lett. 214, 267–277.

Drits, V.A., Lindgreen, H., Sakharov, B.A., Jakobsen, H.J., Salyn, A.L., Dainyak, L.G., 2002. Tobelitization of smectite during oil generation in oil-source shales. Application to north sea illite-tobelite-smectite-vermiculite. Clay Clay Miner. 50, 82–98.

Ducloux, J., Meunier, A., Velde, B., 1976. Smectite, chlorite and a regular interlayered chlorite-vermiculite in soils developed on a small serpentinite body, Massif Central France. Clay Miner. 11, 121–135.

Dupont-Nivet, G., Butler, R.F., Yin, A., Chen, X.H., 2003. Paleomagnetism indicates no Neogene vertical axis rotations of the northeastern Tibetan Plateau. J. Geophys. Res. Solid Earth 108 (B8) (#2386, 19 pp).

Dupont-Nivet, G., Horton, B.K., Zhou, J., Waanders, G.L., Butler, R.F., Wang, J., 2004. Paleogene clockwise tectonic rotation of the Xining-Lanzhou region, northeastern Tibetan Plateau. J. Geophys. Res. Solid Earth 109 (B04401) (13 pp).

Dupont-Nivet, G., Krijgsman, W., Langereis, C.G., Abels, H.A., Dai, S., Fang, X.M., 2007. Tibetan plateau aridification linked to global cooling at the Eocene-Oligocene transition. Nature 445, 635–638.

Dupont-Nivet, G., Hoorn, C., Konert, M., 2008a. Tibetan uplift prior to the Eocene-Oligocene climate transition: evidence from pollen analysis of the Xining Basin. Geology 36, 987–990.

Dupont-Nivet, G., Dai, S., Fang, X.M., Krijgsman, W., Erens, V., Reitsma, M., Langereis, C., 2008b. Timing and distribution of tectonic rotations in the northeastern Tibetan Plateau. In: Burchfiel, B.C., Wang, E. (Eds.), Investigations into the Tectonics of the Tibetan Plateau: Geol. Soc. London, Spec. Publ. 444. pp. 73–87.

Escutia, C., De Santis, L., Donda, F., Dunbar, R.B., Cooper, A.K., Brancolini, G., Eittreim, S.L., 2005. Cenozoic ice sheet history from East Antarctic Wilkes Land continental margin sediments. Glob. Planet. Chang. 45, 51–81.

Fang, X.M., Garzione, C., Van der Voo, R., Li, J.J., Fan, M.J., 2003. Flexural subsidence by 29 Ma on the NE edge of Tibet from the magnetostratigraphy of Linxia Basin, China. Earth Planet. Sci. Lett. 210, 545–560.

Fang, X.M., Yan, M.D., Van der Voo, R., Rea, D.K., Song, C.H., Parés, J.M., Gao, J.P., Nie, J.S., Dai, S., 2005. Late Cenozoic deformation and uplift of the NE Tibetan Plateau: evidence from high-resolution magnetostratigraphy of the Guide Basin, Qinghai Province, China. Geol. Soc. Am. Bull. 117, 1208–1225.

Fedo, C.M., Nesbitt, H.W., Young, G.M., 1995. Unraveling the effects of potassium metasomatism in sedimentary rocks and paleosols, with implications for paleoweathering conditions and provenance. Geology 23, 921–924.

Flower, B.P., Kennett, J.P., 1994. The middle Miocene climatic transition: East Antarctic ice sheet development, deep ocean circulation and global carbon cycling. Palaeogeogr. Palaeoclimatol. Palaeoecol. 108, 537–555.

Fralick, P.W., Kronberg, B.I., 1997. Geochemical discrimination of clastic sedimentary rock sources. Sediment. Geol. 113, 111–124.

Garzione, C.N., Ikari, M.J., Basu, A.R., 2005. Source of Oligocene to Pliocene sedimentary rocks in the Linxia basin in northeastern Tibet from Nd isotopes: implications for tectonic forcing of climate. Geol. Soc. Am. Bull. 117, 1156–1166.

George, A.D., Marshallsea, S.J., Wyrwoll, K., Chen, J., Lu, Y., 2001. Miocene cooling in the northern Qilian Shan, northeastern margin of the Tibetan Plateau, revealed by apatite fission-track and vitrinite-reflectance analysis. Geology 29, 939–942.

Ghandour, I.M., Masuda, H., Maejima, W., 2003. Mineralogical and chemical characteristics of Bajocian-Bathonian shales, G. Al-Maghara, North Sinai, Egypt: climatic and environmental significance. Geochem. J. 37, 87–108.

Gradstein, F.M., Ogg, J.G., Schmitz, M.D., Ogg, G.M., 2012. The Geologic Time Scale 2012. Vol. 606. Cambridge University, Press, Cambridge, UK, pp. 85–113.

Grim, R.E., 1968. Clay Mineralogy. McGraw-Hill, New York (600 pp).

Guo, Z.T., Ruddiman, W.F., Hao, Q.Z., Wu, H.B., Qiao, Y.S., Zhu, R.X., Peng, S.Z., Wei, J.J., Yuan, B.Y., Liu, T.S., 2002. Onset of Asian desertification by 22 Myr ago inferred from loess deposits in China. Nature 416, 159–163.

Guo, Z.T., Sun, B., Zhang, Z.S., Peng, S.Z., Xiao, G.Q., Ge, J.Y., Hao, Q.Z., Qiao, Y.S., Liang, M.Y., Liu, J.F., Yin, Q.Z., 2008. A major reorganization of Asian climate by the early Miocene. Clim. Past 4 (3), 153–174.

Harrison, T., Copeland, P., Kidd, W.S.F., Yin, A., 1992. Raising Tibet. Science 255, 1663–1670.

Hong, H.L., Li, Z.H., Xue, H.J., Zhu, Y.H., Zhang, K.X., Xiang, S.Y., 2007. Oligocene clay mineralogy of the Linxia Basin: evidence of paleoclimatic evolution subsequent to the initial-stage uplift of the Tibetan Plateau. Clay Clay Miner. 55, 492–505.

Hong, H.L., Zhang, K.X., Li, Z.H., 2010. Climatic and tectonic uplift evolution since ~7 Ma in Gyirong basin, southwestern Tibet plateau: clay mineral evidence. Int. J. Earth Sci. 99, 1305–1315.

Horton, B.K., Dupont-Nivet, G., Zhou, J., Waanders, G.L., Butler, R.F., Wang, J., 2004. Mesozoic-Cenozoic evolution of the Xining-Minhe and Dangchang basins, northeastern Tibetan Plateau: magnetostratigraphic and biostratigraphic results. J. Geophys. Res. Solid Earth 109 (B04402) (15 pp).

Hough, B.G., Garzione, C.N., Wang, Z.C., Lease, R.O., Burbank, D.W., Yuan, D.Y., 2011. Stable isotope evidence for topographic growth and basin segmentation: implications for the evolution of the NE Tibetan Plateau. Geol. Soc. Am. Bull. 123, 168–185.

Hurlbut, C.S., Klein, C., 1985. Manual of Mineralogy. Wiley, New York (324 pp).

Ji, J., Zhang, K., Qiang, T., Kou, X., Chen, F., Xu, Y., Lu, J., Lin, Q., 2010. Magnetostratigraphy of the Neogene Strata in Xunhua Basin, Qinghai Province. Earth Sci. J. China Univ. Geosci. 35, 803–810 (in Chinese).

Jiang, H.C., Ding, Z.L., 2008. A 20 Ma pollen record of East-Asian summer monsoon evolution from Guyuan, Ningxia, China. Palaeogeogr. Palaeoclimatol. Palaeoecol. 265, 30–38.

Jiang, H.C., Ding, Z.L., Xiong, S.F., 2007. Magnetostratigraphy of the Neogene Sikouzi section at Guyuan, Ningxia, China. Palaeogeogr. Palaeoclimatol. Palaeoecol. 243, 223–234.

Jiménez-Morenoa, G., Rodríguez-Tovara, F.J., Pardo-Igúzquizac, U., Fauquetted, S., Suc, J.P., Müller, P., 2005. High-resolution palynological analysis in late early-middle Miocene core from the Pannonian Basin, Hungary: climatic changes, astronomical forcing and eustatic fluctuations in the Central Paratethys. Palaeogeogr. Palaeoclimatol. Palaeoecol. 216, 73–97.

Jolivet, M., Brunel, M., Seward, D., Xu, Z., Yang, J., Roger, F., Tapponnier, P., Malavieille, J., Leyreloup, A., Arnaud, N., Wu, C., 2001. Mesozoic and Cenozoic tectonics of the northern edge of the Tibetan plateau: fission-track constraints. Tectonophysics 343, 111–134.

Kahle, M., Kleber, M., Jahn, R., 2002. Review of XRD-based quantitative analyses of clay minerals in soils: the suitability of mineral intensity factors. Geoderma 109, 191–205.

Lease, R.O., Burbank, D.W., Gehrels, G.E., Wang, Z.C., Yuan, D.Y., 2007. Signatures of mountain building: detrital zircon U/Pb ages from northeastern Tibet. Geology 35, 239–242.

Lease, R.O., Burbank, D.W., Clark, M.K., Farley, K.A., Zheng, D., Zhang, H., 2011. Middle Miocene reorganization of deformation along the northeastern Tibetan Plateau. Geology 39, 359–362.

Lease, R.O., Burbank, D.W., Hough, B., Wang, Z., Yuan, D., 2012. Pulsed Miocene range growth in northeastern Tibet: insights from Xunhua Basin magnetostratigraphy and provenance. Geol. Soc. Am. Bull. 124, 657–677.

Li, J.J., Fang, X.M., Van der Voo, R., Zhu, J.J., Niocaill, C.M., Cao, J.X., Zhong, W., Chen, H.L., Wang, J.L., Wang, J.M., Zhang, Y.C., 1997. Late cenozoic magnetostratigraphy (11–0 Ma) of the Dongshanding and Wangjiashan sections in the Longzhong Basin, western China. Geol. Mijnb. 76, 121–134.

Liu, T.S., Ding, Z.L., 1998. Chinese loess and the paleomonsoon. Annu. Rev. Earth Planet. Sci. 26, 111–145.

Liu, S.F., Zhang, G.W., Heller, P.L., 2007. The development of Cenozoic basins in Xunhua-Guide area and its indication of plateau uplift. Sci. China D Earth Sci. S1, 235–248 (in Chinese).

Liu, Y.S., Zong, K.Q., Kelemen, P.B., Gao, S., 2008. Geochemistry and magmatic history of eclogites and ultramafic rocks from the Chinese continental scientific drill hole: subduction and ultrahigh-pressure metamorphism of lower crustal cumulates. Chem. Geol. 247, 133–153.

Lu, H.Y., Wang, X.Y., An, Z.S., Miao, X.D., Zhu, R.X., Ma, H.Z., Li, Z., Tan, H.B., Wang, X.Y., 2004. Geomorphologic evidence of phased uplift of the northeastern Qinghai-Tibet Plateau since 14 million years ago. Sci. China D: Earth Sci. 47, 822–833.

Ma, Y.Z., Li, J.J., Fang, X.M., 1998. Pollen assemblage in 30.6–5.0 Ma redbeds of Linxia region and climate evolution. Chin. Sci. Bull. 43, 301–304 (in Chinese).

Manabe, S., Terpstra, T.B., 1974. The effects of mountains on the general circulation of the atmosphere as identified by numerical experiments. J. Atmos. Sci. 31, 3–42.

McLennan, S.M., 1993. Weathering and global denudation. J. Geol. 101, 295–303.

Miao, Y.F., Herrmann, M., Wu, F.L., Yan, X.L., Yang, S.L., 2012. What controlled Mid-Late Miocene long-term aridification in Central Asia? –global cooling or Tibetan Plateau uplift: a review. Earth Sci. Rev. 112, 155–172.

Miller, K.G., Kominz, M.A., Browning, J.V., Wright, J.D., Mountain, G.S., Katz, M.E., Sugarman, P.J., Cramer, B.S., Christie-Blick, N., Pekar, S.F., 2005. The phanerozoic record of global sea-level change. Science 310, 1293–1298.
Mock, C., Arnaud, N.O., Cantagrel, J.M., 1999. An early unroofing in northeastern Tibet? Constraints from $^{40}Ar/^{39}Ar$ thermochronology on granitoids from the eastern Kunlun range (Qianghai, NW China). Earth Planet. Sci. Lett. 171, 107–122.
Molnar, P., Stock, J.M., 2009. Slowing of India's convergence with Eurasia since 20 Ma and its implications for Tibetan mantle dynamics. Tectonics 28, TC3001 (11 pp).
Molnar, P., Tapponnier, P., 1975. Cenozoic tectonics of Asia: effects of a continental collision. Science 189, 419–426.
Molnar, P., England, P., Joseph, M., 1993. Mantle dynamics, uplift of the Tibetan plateau, and the Indian monsoon. Rev. Geophys. 31, 357–396.
Molnar, P., Boos, W.R., Battisti, D.S., 2010. Orographic controls on climate and paleoclimate of Asia: thermal and mechanical roles for the Tibetan Plateau. Annu. Rev. Earth Planet. Sci. 38, 77–102.
Moore, D.M., Reynolds, R.C., 1989. X-ray Diffraction and the Identification and Analysis of Clay Minerals. Oxford University Press, Oxford (332 pp).
Nesbitt, H.W., Young, G.M., 1982. Early Proterozoic climates and plate motions inferred from major element chemistry of lutites. Nature 299, 715–717.
Parés, J.M., Van der Voo, R., Downs, W.R., Yan, M., Fang, X., 2003. Northeastward growth and uplift of the Tibetan Plateau: magnetostratigraphic insights from the guide Basin. J. Geophys. Res. Solid Earth 108 (B1), 2017 (11 pp).
Perry, E.A., Hower, J., 1970. Burial diagenesis in Gulf Coast politic sediments. Clay Clay Miner. 18, 165–177.
Ramstein, G., Fluteau, F., Besse, J., Joussaume, S., 1997. Effect of orogeny, plate motion and land-sea distribution on Eurasian climate change over the past 30 million years. Nature 386, 788–795.
Robert, C., Kennett, J.P., 1994. Antarctic subtropical humid episode at the Paleocene-Eocene boundary: clay-mineral evidence. Geology 22, 211–214.
Robert, C., Kennett, J.P., 1997. Antarctic continental weathering changes during Eocene-Oligocene cryosphere expansion: clay mineral and oxygen isotope evidence. Geology 25, 587–590.
Ruddiman, W.F., Kutzbach, J.E., 1989. Forcing of late Cenozoic Northern Hemisphere climate by plateau uplift in southern Asia and the American West. J. Geophys. Res.-Atmos. 94 (D15), 18409–18427.
Sobel, E.R., Dumitru, T.A., 1997. Thrusting and exhumation around the margins of the western Tarim basin during the India-Asia collision. J. Geophys. Res. Solid Earth 102 (B3), 5043–5063.
Sobel, E.R., Chen, J., Heermance, R.V., 2006. Late Oligocene–Early Miocene initiation of shortening in the Southwestern Chinese Tian Shan: implications for Neogene shortening rate variations. Earth Planet. Sci. Lett. 247, 70–81.
Song, C.H., Fang, X.M., Gao, J.P., Nie, J.S., Yan, M., Xu, X.H., 2003. Magnetostratigraphy of Late Cenozoic fossil mammals in the northeastern margin of the Tibetan plateau. Chin. Sci. Bull. 48, 188–193.
Spicer, R.A., Harris, N.B.W., Widdowson, M., Herman, A.B., Guo, S., Valdes, P.J., Wolfek, J.A., Kelley, S.P., 2003. Constant elevation of southern Tibet over the past 15 million years. Nature 412, 622–624.
Sun, X.J., Wang, P.X., 2005. How old is the Asian monsoon system?–Palaeobotanical records from China. Palaeogeogr. Palaeoclimatol. Palaeoecol. 222, 181–222.
Sun, J., Zhang, Z., 2008. Palynological evidence for the Mid-Miocene climatic optimum recorded in Cenozoic sediments of the Tian Shan Range, northwestern China. Glob. Planet. Chang. 64, 53–68.
Tang, Z.H., Ding, Z.L., White, P.D., Dong, X.X., Ji, J.L., Jiang, H.C., Luo, P., Wang, X., 2011. Late Cenozoic central Asian drying inferred from a palynological record from the northern Tian Shan. Earth Planet. Sci. Lett. 302, 439–447.
Tapponnier, P., Xu, Z., Roger, F., Meyer, B., Arnaud, N., Wittlinger, G., Yang, J., 2001. Oblique stepwise rise and growth of the Tibet Plateau. Science 294, 1671–1677.
Turner, S., Hawkesworth, C., Liu, J.Q., Rogers, N., Kelley, S., Vancalsteren, P., 1993. Timing of Tibetan uplift constrained by analysis of volcanic rocks. Nature 364, 50–54.
Utescher, T., Mosbrugger, V., Ashraf, A., 2000. Terrestrial climate evolution in Northwest Germany over the last 25 million years. PALAIOS 15, 430–449.
Vanderaveroet, P., 2000. Miocene to Pleistocene clay mineral sedimentation on the New Jersey shelf. Oceanol. Acta 23, 25–36.
Vicente, M.A., Elsass, F., Molina, E., Robert, M., 1997. Palaeoweathering in slates from the Iberian Hercynian. Massif (Spain): investigation by TEM of clay mineral signatures. Clay Miner. 32, 435–451.
Wang, E., 2013. Evolution of the Tibetan Plateau: as constrained by major tectonic-thermo events and a discussion on their origin. Sci. Geol. Sin. 48, 334–353 (in Chinese).
Wang, C.W., 2015. Clay Mineralogical Characteristics of the Cenozoic Sediments from the Northern Qinghai-Tibetan Plateau: Indictors for Tectonic and Climatic Evolution. Ph.D. Thesis. China University of Geosciences, Wuhan, China (in Chinese).
Wang, Y., Deng, T., 2005. A 25 m.y. isotopic record of paleodiet and environmental change from fossil mammals and paleosols from the NE margin of the Tibetan Plateau. Earth Planet. Sci. Lett. 236, 322–338.
Wang, C.W., Zhao, X., Liu, Z., Lippert, P.C., Graham, S.A., Coe, R.S., Yi, H., Zhu, L., Liu, S., Li, Y., 2008a. Constraints on the early uplift history of the Tibetan Plateau. Proc. Natl. Acad. Sci. U. S. A. 105, 4987–4992.
Wang, S.F., Zhang, W.L., Fang, X.M., Dai, S., Oliver, K., 2008b. Magnetostratigraphy of the Zanda basin in Southwest Tibet plateau and its tectonic implications. Chin. Sci. Bull. 53, 1393–1400.
Wang, W., Zhang, P., Kirby, E., Wang, L., Zhang, G., Zheng, D., Chai, C., 2011. A revised chronology for Tertiary sedimentation in the Sikouzi basin: implications for the tectonic evolution of the northeastern corner of the Tibetan Plateau. Tectonophysics 505, 100–114.
Wang, C.W., Hong, H., Li, Z., Liang, G., Xie, J., Song, B., Song, E., Zhang, K., 2013a. Climatic and tectonic evolution in the North Qaidam since the Cenozoic: evidence from sedimentology and mineralogy. J. Earth Sci. 24, 314–327.
Wang, C.W., Hong, H., Li, Z., Yin, K., Xie, J., Liang, G., Song, B., Song, E., Zhang, K., 2013b. The Eocene-Oligocene climate transition in the Tarim Basin, Northwest China: evidence from clay mineralogy. Appl. Clay Sci. 74, 10–19.
Warr, L.N., Rice, A.H.N., 1994. Interlaboratory standardization and calibration of day mineral crystallinity and crystallite size data. J. Metamorph. Geol. 12, 141–152.
Warren, J., 2000. Dolomite: occurrence, evolution and economically important associations. Earth-Sci. Rev. 52, 1–81.
West, J.M., Pearce, J., Bentham, M., Maul, P., 2005. Issue profile: environmental issues and the geological storage of CO_2. Eur. Environ. 15, 250–259.
Xiao, G.Q., Guo, Z., Dupont-Nivet, G., Lu, H., Wu, N., Ge, J., Hao, Q., Peng, S., Li, F., Abels, H.A., Zhang, K., 2012. Evidence for northeastern Tibetan Plateau uplift between 25 and 20 Ma in the sedimentary archive of the Xining Basin, Northwestern China. Earth Planet. Sci. Lett. 317-318, 185–195.
Xiong, S., Ding, Z., Zhu, Y., Zhou, R., Lu, H., 2010. A ~6 Ma chemical weathering history, the grain size dependence of chemical weathering intensity, and its implications for provenance change of the Chinese loess-red clay deposit. Quat. Sci. Rev. 29, 1911–1922.
Xu, Z.L., 2015. Oligocene-Miocene Pollen Records in Xunhua Basin, Northeastern Tibetan Plateau and its Implications for Evolution of the East Asian Monsoon. Ph.D. Thesis. China University of Geosciences, Wuhan, China (in Chinese).
Xu, Z.L., Zhang, J.Y., Ji, J.L., Zhang, K.X., 2015. The mid-Miocene pollen record of the Xunhua Basin, NE Tibetan Plateau: Implications for global climate change. Acta Geol. Sin. 89, 1649–1663.
Ye, H., Zhang, K.X., Ji, J.L., Liang, M.Y., Zhang, J.Y., Xu, Y.D., Chen, F.N., 2010. Major and trace element characters of the sediments and paleoclimatic evolvement during about 23.1–5.0 Ma in Xunhua Basin, Qinghai. J. Earth Sci. 35, 811–820 (in Chinese).
Yin, A., Nie, S., Craig, P., Harrison, T.M., 1998. Late Cenozoic tectonic evolution of the southern Chinese Tian Shan. Tectonics 17, 1–27.
Yin, A., Dang, Y., Zhang, M., McRivette, M.W., Burgess, W.P., Chen, X., 2007. Cenozoic tectonic evolution of Qaidam basin and its surrounding regions (part 2): wedge tectonics in southern Qaidam basin and the Eastern Kunlun Range. Geol. Soc. Am. Bull. 433, 369–390.
Yin, K., Hong, H.L., Li, R.B., Xu, Y.M., Du, J., Ji, J.L., Zhang, K.X., 2010a. Clay mineralogy and its palaeoclimatic indicator of the late Oligocene and early Miocene in Xunhua Basin. Geol. Sci. Technol. Inf. 29, 41–48 (in Chinese).
Yin, K., Hong, H.L., Li, R.B., Qiang, T., Zhang, K.X., Wang, J.R., 2010b. Characteristics of clay mineralogy of late Oligocene sediments in Xunhua Basin, Qinghai Province and their implications for paleoclimate. GeoSci. 24, 187–194 (in Chinese).
Yin, K., Hong, H.L., Churchman, G.J., Li, R.B., Li, Z.H., Wang, C.W., Han, W., 2013. Hydroxy-interlayered vermiculite genesis in Jiujiang late-Pleistocene red earth sediments and significance to climate. Appl. Clay Sci. 74, 20–27.
Yue, L.P., Heller, F., Qiu, Z.X., Zhang, L., Xie, G.P., Qiu, Z.D., Zhang, Y.X., 2001. Magnetostratigraphy and paleoenvironmental record of tertiary deposits of Lanzhou Basin. Chin. Sci. Bull. 46, 770–773.
Yue, L.P., Deng, T., Zhang, R., Zhang, Z.Q., Heller, F., Wang, J.Q., Wang, L.R., 2004. Paleomagnetic chronology and records of Himalayan uplift on the Longgugou section of Gyirong-Oma Basin in Xizhang (Tibet). Chin. J. Geophys. 47, 1009–1016 (in Chinese).
Zachos, J.C., Pagani, M., Sloan, L., Thomas, E., Billups, K., 2001. Trends, rhythms, and aberrations in global climate 65 Ma to present. Science 292, 689–693.
Zachos, J.C., Dickens, G.R., Zeebe, R.E., 2008. An early Cenozoic perspective on greenhouse warming and carbon-cycle dynamics. Nature 451, 279–283.
Zhang, C., Wang, L., Li, G., Dong, S., Yang, J., Wang, X., 2002. Grain size effect on multi-element concentrations in sediments from the intertidal flats of Bohai Bay, China. Appl. Geochem. 17, 59–68.
Zhang, Z.S., Wang, H.J., Guo, Z.T., Jiang, D.B., 2007a. Impacts of tectonic changes on the reorganization of the Cenozoic paleoclimatic patterns in China. Earth Planet. Sci. Lett. 257, 622–634.
Zhang, Z.S., Wang, H.J., Guo, Z.T., Jiang, D.B., 2007b. What triggers the transition of palaeoenvironmental patterns in China, the Tibetan Plateau uplift or the Paratethys Sea retreat? Palaeogeogr. Palaeoclimatol. Palaeoecol. 245, 317–331.
Zhang, K.X., Wang, G.C., Hong, H.L., Xu, Y.D., Wang, A., Cao, K., Luo, M.S., Ji, J.L., Xiao, G.Q., Lin, X., 2013. The study of the Cenozoic uplift in the Tibetan Plateau: a review. Geol. Bull. China 32, 1–18 (in Chinese).
Zhang, C., Xiao, G., Guo, Z., Wu, H., Hao, Q., 2015. Evidence of late early Miocene aridification intensification in the Xining Basin caused by the northeastern Tibetan Plateau uplift. Glob. Planet. Chang. 128, 31–46.
Zheng, D.W., Zhang, P.Z., Wan, J.L., Li, C.Y., Cao, J.X., 2003. Late Cenozoic deformation subsequence in northeastern margin of Tibet–Detrital AFT records from Linxia Basin. Sci. China D: Earth Sci. 46, 266–275.
Zheng, D.W., Zhang, P.Z., Wan, J.L., Yuan, D.Y., Li, C.Y., Yin, G.M., Zhang, G.L., Wang, Z.C., Min, W., Chen, J., 2006. Rapid exhumation at 8 Ma on the Liupan Shan thrust fault from apatite fission-track thermochronology: implications for growth of the northeastern Tibetan Plateau margin. Earth Planet. Sci. Lett. 248, 198–208.